Deciphering the Roles of MA-Based Volatile Additives for α-$FAPbI_3$ to Enable Efficient Inverted Perovskite Solar Cells

Bi, Leyu; Fu, Qiang; Zeng, Zixin; Wang, Yunfan; Lin, Francis R.; Cheng, Yuanhang; Yip, Hin-Lap; Tsang, Sai Wing; Jen, Alex K.-Y.

Published in:
Journal of the American Chemical Society

Published: 15/03/2023

Document Version:
Post-print, also known as Accepted Author Manuscript, Peer-reviewed or Author Final version

Published version (DOI):
10.1021/jacs.2c13566

Publication details:
Bi, L., Fu, Q., Zeng, Z., Wang, Y., Lin, F. R., Cheng, Y., Yip, H.-L., Tsang, S. W., & Jen, A. K.-Y. (2023). Deciphering the Roles of MA-Based Volatile Additives for *α*-$FAPbI_3$ to Enable Efficient Inverted Perovskite Solar Cells. *Journal of the American Chemical Society*, *145*(10), 5920-5929. https://doi.org/10.1021/jacs.2c13566

Deciphering the roles of MA-based Volatile Additives for α-$FAPbI_3$ Enable Efficient Inverted Perovskite Solar Cells

Leyu Bi,[†,a,b,c] Qiang Fu,[†,a,b,c] Zixin Zeng, [a] Yunfan Wang, [a] Francis R. Lin, [a,b,c] Yuanhang Cheng, [d] Hin-Lap Yip, [a,b,c] Sai-Wing Tsang, [a] and Alex K.-Y. Jen*[a,b,c]

[a]Department of Materials Science and Engineering, City University of Hong Kong Kowloon 999077 (Hong Kong)

[b]Department of Chemistry, City University of Hong Kong, Kowloon 999077 (Hong Kong)

[c]Hong Kong Institute for Clean Energy, City University of Hong Kong, Kowloon 999077 (Hong Kong)

[d] School of New Energy, Nanjing University of Science and Technology, Jiangsu, 214443, (PR China)

[†]These authors contributed equally to this work

*Corresponding author. Email: alexjen@cityu.edu.hk (A.K.Y.J.)

KEYWORDS. Perovskite solar cells, $FAPbI_3$, Volatile additive, Crystallization dynamics, In-situ photoluminescence.

ABSTRACT: Functional additives that can interact with the perovskite precursors to form the intermediate phase have been proven essential in obtaining uniform and stable α-$FAPbI_3$ films. Among them, Cl-based volatile additives are the most prevalent in the literature. However, their exact role is still unclear, especially in inverted perovskite solar cells (PSCs). In this work, we have systematically studied the functions of Cl-based volatile additives and MA-based additives in formamidinium lead iodide ($FAPbI_3$)-based inverted PSCs. Using *in-situ* photoluminescence, we provide clear evidence to unravel the different roles of volatile additives (NH_4Cl, FACl and MACl) and MA-based additives (MACl, MABr and MAI) in the nucleation, crystallization, and phase transition of $FAPbI_3$. Three different kinds of crystallization routes are proposed based on the above additives. The non-MA volatile additives (NH_4Cl and FACl) were found to promote crystallization and lower the phase transition temperatures. The MA-based additives could quickly induce MA-rich nuclei to form pure α-phase $FAPbI_3$ and dramatically reduce phase transition temperatures. Furthermore, volatile MACl provides a unique effect on promoting the growth of secondary crystallization during annealing. The optimized solar cells with MACl can achieve an efficiency of 23.1%, which is the highest in inverted $FAPbI_3$-based PSCs.

INTRODUCTION

Perovskite solar cells (PSCs) have emerged as a promising technology for the photovoltaic industry owing to their overwhelmingly improved performance and the cost-effective solution processing process. [1-9] Although inverted (*p-i-n* structure) PSCs are attractive for future commercialization due to their low-temperature processability and better compatibility with flexible substrates and perovskite-based tandem device fabrication, [10-15] they typically exhibit lower power conversion efficiency (PCE) than their regular (*n-i-p*) counterparts. [16-18] Most certified-record PCEs are based on single-junction *n-i-p* PSCs using an optimized formamidinium lead triiodide ($FAPbI_3$) perovskite absorber layer. [19-21] However, the excellent performance of $FAPbI_3$ in *n-i-p* PSCs could not be directly translated into efficient inverted PSCs. So far, only a few studies have reported using $FAPbI_3$ in inverted PSCs, and the PCEs are usually below 22%. [22-23] The main bottleneck limiting the PCE of $FAPbI_3$-based inverted PSCs is the needed high-temperature phase transition (⩾150 °C) for forming α-phase $FAPbI_3$, which is detrimental to inverted PSCs. [23]

To overcome this problem, a widely used strategy in inverted PSCs is compositional engineering by alloying $FAPbI_3$ with a small fraction of non-native cations, such as Cs^+, MA^+ and Rb^+ cation, and Br^- anion, as used in most state-of-the-art PSCs. [10-12, 24-25] However, tuning of compositions will inevitably increase the bandgap and suffer from possible local phase segregation of non-native cations and halides. [26] Therefore, instead of using a substitution strategy, volatile additives have been incorporated in the perovskite precursor solution to form pure black-phase α-$FAPbI_3$ perovskite film and increase crystallinity. [21, 27-28]

To facilitate the crystallization and phase transition at relatively low temperatures, the additives are expected to coordinate with the Pb atom in the precursor and be easily released during the film annealing process. [26] In this regard, small-volume cations with amino groups are good candidates for volatile additives. Besides, chloride additives have been proven to effectively promote perovskite crystallization, which is conducive to perovskite morphology and film quality. [29-30] Therefore, several volatile additives such as ammonium chloride (NH_4Cl), [31-32] methylamine chloride (MACl) [21, 33] and formamidine chloride

(FACl) [28] have been applied to facilitate the crystallization and phase transition of α-FAPbI3. However, the guideline for choosing the most suitable additive and understanding how additives affect the nucleation and crystallization of α-FAPbI3 are still unclear. [34]

Therefore, we have systematically studied the roles of volatile additives (NH_4Cl, FACl and MACl) and MA-based additives (MACl, MABr and MAI) in nucleation, crystallization, and phase transition of $FAPbI_3$ by using in-situ photoluminescence (PL). This work revealed three different kinds of $FAPbI_3$ crystallization routes, which could provide helpful guidance for choosing appropriate additives to achieve high-performance inverted PSC. We found that non-MA volatile additives (NH_4Cl and FACl) could promote crystallization and lower the phase transition temperatures. MA-based additives could quickly induce MA-rich nuclei to facilitate the formation of α-phase $FAPbI_3$ and dramatically reduce phase transition temperatures. Furthermore, MACl could combine benefits from volatile and MA-containing additives to promote secondary crystallization during annealing, as revealed in the in-situ PL. With the above understanding, the optimized solar cells with MACl could be fabricated to achieve 23.1% efficiency, which is one of the best in FAPbI3-based inverted PSCs.

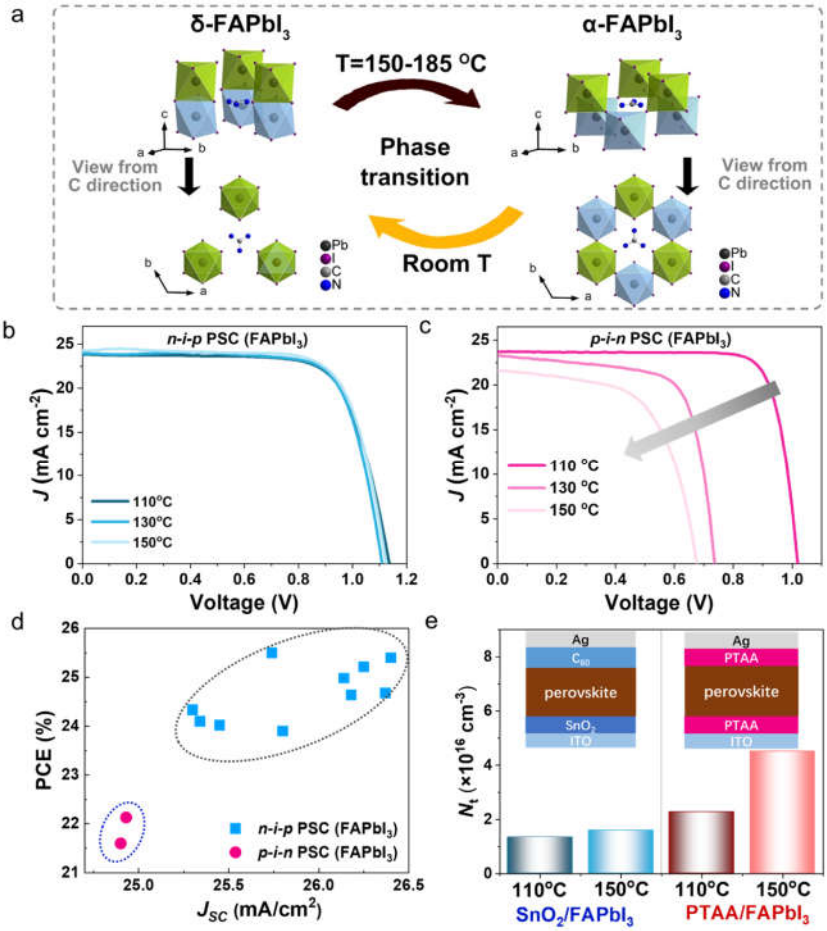

Figure 1. (a) Crystalline structures viewed from different directions showing δ-$FAPbI_3$ and α-$FAPbI_3$ phases and the phase transition between them. Three [PbI_6] octahedra in the upper or lower layer are labeled green or blue, respectively. The view of δ-$FAPbI_3$ from the C direction shows two overlapped layers, while in the case of α-$FAPbI_3$, it shows crossed structure between two layers. Pb, I, C and N atoms are labeled deep grey, purple, grey, and blue. (b, c) *J-V* curves evolution of (b) *n-i-p* and (c) *p-i-n* structured PSCs with the different annealing temperatures. (d) Recent advances in efficient $FAPbI_3$-based PSCs in *n-i-p* or *p-i-n* structures. (e) Defect density from SCLC measurement of $FAPbI_3$ based on SnO_2 or PTAA substrates annealed at different temperatures.

RESULTS AND DISCUSSION

As shown in **Figure 1a**, the photoactive black α-phase $FAPbI_3$ perovskite is thermodynamically unstable, which will spontaneously transform into a photo-inactive δ-phase at room temperature, especially in humid ambient air. [35] During the crystallization of $FAPbI_3$, α and δ-phase $FAPbI_3$ are formed simultaneously, and δ-$FAPbI_3$ will undergo a reversible phase transition to α-$FAPbI_3$ when the temperature rises above 150 °C. [35] To gain a thorough understanding of the lattice and ionic changes between δ-$FAPbI_3$ and α-$FAPbI_3$ during the reversible phase transition, the single-crystal structure data of δ-$FAPbI_3$ and α-$FAPbI_3$ were further analyzed. **Figure 1a** shows different views of the lattice structure in δ-$FAPbI_3$ and α-$FAPbI_3$, suggesting that

the phase transition between δ-$FAPbI_3$ and α-$FAPbI_3$ may arise from the movement of ions between adjacent layers.

Detailed analysis and discussion are shown in **Figure S1-S3**. Encouragingly, significant progress has been made toward stabilizing α-$FAPbI_3$ without changing the bandgap, which significantly led to the recent ascending of PCE for $FAPbI_3$-based regular PSCs over 25% [16-17, 19-21, 27, 36-40] (**Figure 1d**). However, the PCE of $FAPbI_3$-based inverted PSCs was still less than 22% [22-23, 41], far behind that of the regular PSCs. The regular and inverted-structured PSCs adopt different substrate materials for perovskite deposition, which might be a critical reason for their remarkably different photovoltaic performance. Therefore, we compared regular and inverted-structured PSCs based on the one-step deposition of $FAPbI_3$ films to study their potential variations. The details on device fabrication can be seen in supporting information. We found that the annealing process of $FAPbI_3$ perovskite films on HTL substrates significantly differed from that of regular PSCs. According to the literature, the optimal annealing conditions of $FAPbI_3$ perovskite on inorganic electron-transporting layers like TiO_2 or SnO_2 is heating at 150 °C for 10–20 min. However, the same fabrication conditions resulted in deficient photovoltaic performance for inverted structured PSCs (**Figure 1b, c**).

Therefore, we have systematically optimized the annealing conditions by decreasing the annealing temperature from 150 to 130 to 110 °C. The detailed photovoltaic parameters were compared in **Table S2**. Intriguingly, we found that the photovoltaic performance of $FAPbI_3$-based inverted PSCs could be improved upon decreasing the annealing temperature of perovskite films, and the best results were obtained at 110 °C. However, the performance of the regular PSC using different annealing temperatures remained unchanged. To clarify the considerable difference, we studied the morphology and crystallinity of $FAPbI_3$ films on PTAA and SnO_2 annealed at 110 and 150 °C, respectively. From the X-ray diffraction (XRD) and scanning electron microscopy (SEM) measurements (**Figure S5-S6**), the PTAA substrates seemed not to change the properties of $FAPbI_3$ perovskite films at high annealing temperature compared with SnO_2.

The trap density of $FAPbI_3$ films based on PTAA or SnO_2 was further evaluated by the space charge-limited current (SCLC) measurements based on hole-only devices with the structure of ITO/PTAA/$FAPbI_3$/PTAA/Ag or electron-only devices with the structure of ITO/ SnO_2/$FAPbI_3$/C60/Ag. [42-43] As shown in **Figure 1e** and **S7**, the trap density of $FAPbI_3$ coated on SnO_2 was 1.34×10^{16} cm^{-3}, and 1.56×10^{16} cm^{-3} for samples after being annealed at 110 ℃ and 150 ℃, which only shows a slightly increased trap density. However, the $FAPbI_3$ coated on PTAA annealed at 150 °C and 110 °C showed higher trap densities of 2.27×10^{16} cm^{-3} and 4.51×10^{16} cm^{-3}. The gap between them is much larger than that for the SnO_2 substrate, indicating that the annealing process at 150 °C might promote more interface defects in inverted devices. NiO_x and SAM-based substrates also show a similar increased defect density at 150 °C as shown in **Figure S7.** Therefore, effectively reducing the temperature of phase transition and thermal annealing to achieve α-$FAPbI_3$ may be the key to improving the PCE of $FAPbI_3$-based inverted PSCs.

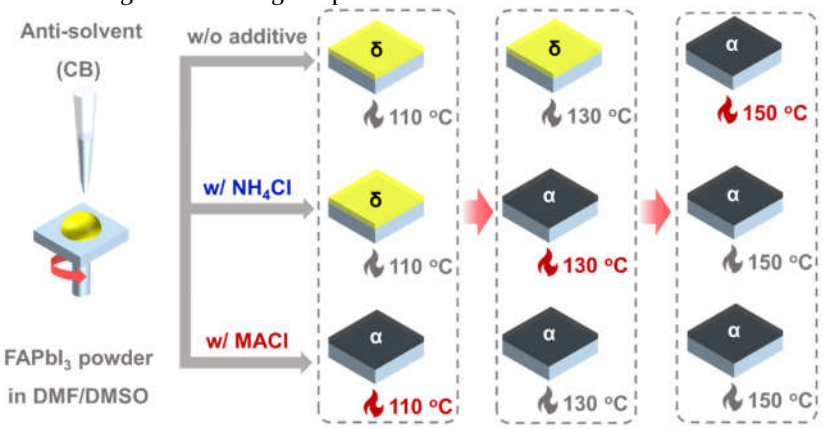

Scheme 1. Schematic diagram of $FAPbI_3$ films for control and with NH_4Cl or MACl under different annealing temperatures.

Additive engineering is a common strategy for controlling the crystal phase and surface morphology of perovskite films. [21, 26] To study the underlying mechanism of how additives affect the crystallization of α-$FAPbI_3$ and guide for choosing appropriate additives, NH_4Cl and MACl were selected as the main volatile additives to study their effects on the $FAPbI_3$ crystallization and phase transition. The precursor solution was prepared by dissolving selected additives and $FAPbI_3$ powder into DMF/DMSO mixed solvent. As shown in **Scheme 1** and **Figure S8-S9**, photos of perovskite films were taken after annealing at different temperatures, where the phase transition was further confirmed by XRD measurements. We found that the film with NH_4Cl had a lower phase transition temperature (130 °C) than that without additives (150 °C). Moreover, the film with MACl could achieve the phase transition below 110 °C (even at 60 °C), which indicated that MACl could more effectively promote the formation of α-$FAPbI_3$.

To further investigate the roles of additives in $FAPbI_3$ formation, *in-situ* photoluminescence (PL) measurements were conducted to monitor the $FAPbI_3$ perovskite crystallization process as shown in **Figure 2a**. After the precursor solution was spin-coated onto a glass substrate, the sample was immediately transferred to a hot plate and monitored by *in-situ* PL. The annealing process was performed under different temperatures according to the phase transition

temperature described in **Scheme 1**. **Figure 2b-2d** and Figure **S11**, **S12**, **S14** show the heat maps of the PL spectra for $FAPbI_3$, w/NH_4Cl, and w/MACl taken during the annealing process.

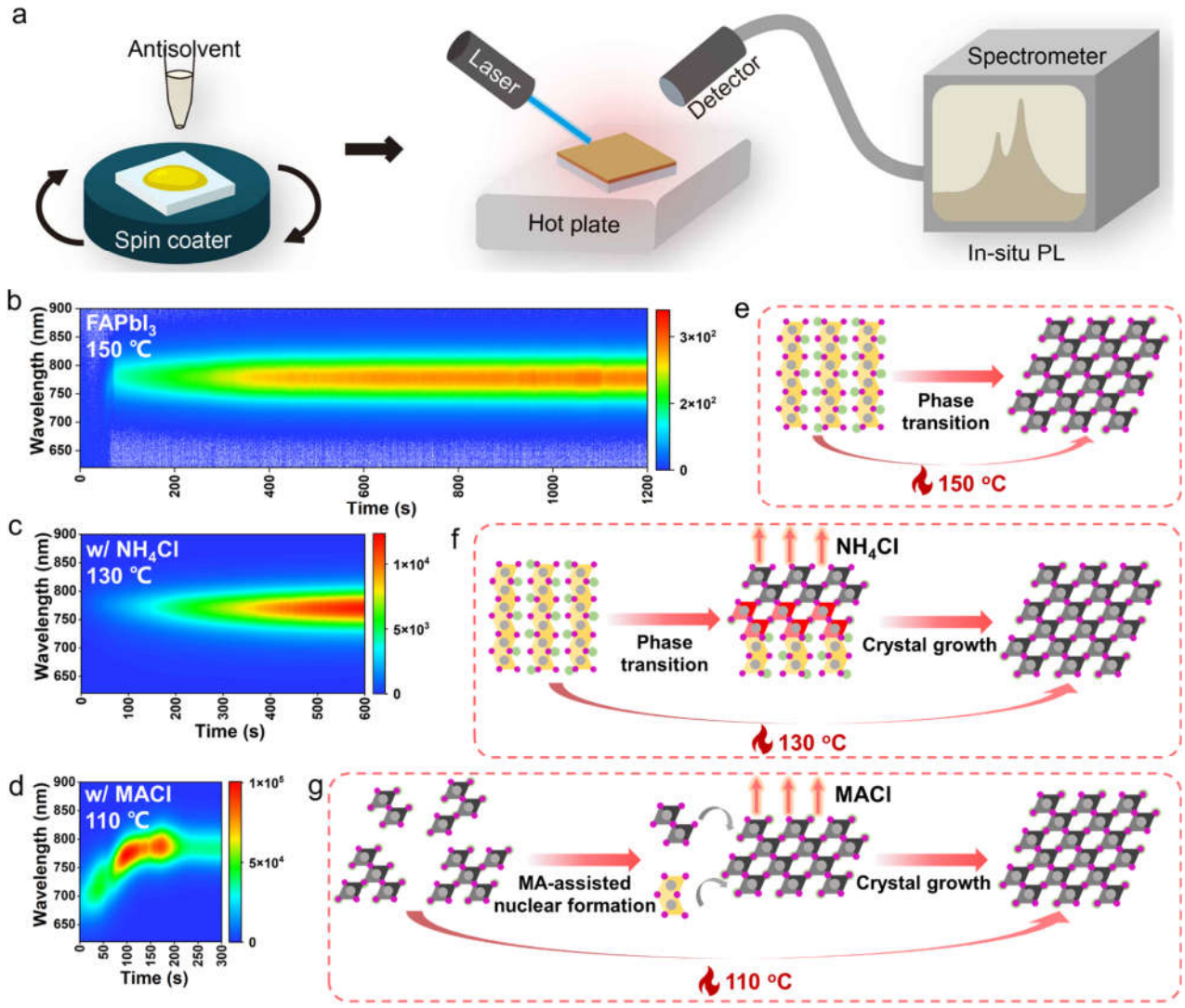

Figure 2. (a) Schematic illustration of in-situ photoluminescence (PL) monitoring during the $FAPbI_3$ perovskite crystallization. (b, c, d) Heat maps of in-situ PL of $FAPbI_3$ film under the different annealing temperatures for (b) control, (c) with NH_4Cl and (d) with MACl. (e, f, g) Schematic illustration for crystallization kinetics of different phase transition and crystallization routes to α-$FAPbI_3$ film through thermal annealing or volatile additive-assisted crystallization under the various annealing temperatures for (e) control, (f) with NH_4Cl and (g) with MACl.

The shifts of the PL peaks in **Figure 2b and S11** showed that the $FAPbI_3$ sample reached its maximum PL intensity of 3×10^2 when heated at 150°C for 150s. The introduction of NH_4Cl reduced the phase transition temperature to below 130°C and enhanced the maximum PL intensity by two orders of magnitude to 1.3×10^4, indicating the improved crystallinity and film quality of $FAPbI_3$. Note that volatile FACl also had a similar effect to NH_4Cl, as shown in **Figure S10**. Unlike the first two crystallization routes, the sample with MA-based volatile additive MACl had a faster crystallization rate. It reached the maximum PL intensity (1×10^5), which was one more order of magnitude higher than that for the NH_4Cl sample, showing further increased crystallization rate and film crystallinity. Moreover, different from NH_4Cl and FACl, the maximum PL peak position of the MACl-based sample gradually shifted from 700 nm to 780 nm during the first 100s of annealing. This significant peak shift may be attributed to MACl-assisted nucleation, which dramatically reduced the phase-transition temperature and simultaneously increased the speed of forming α-phase $FAPbI_3$. Based on our observations, we show a schematic diagram of possible crystallization kinetics, as shown in **Figure 2e-2g**.

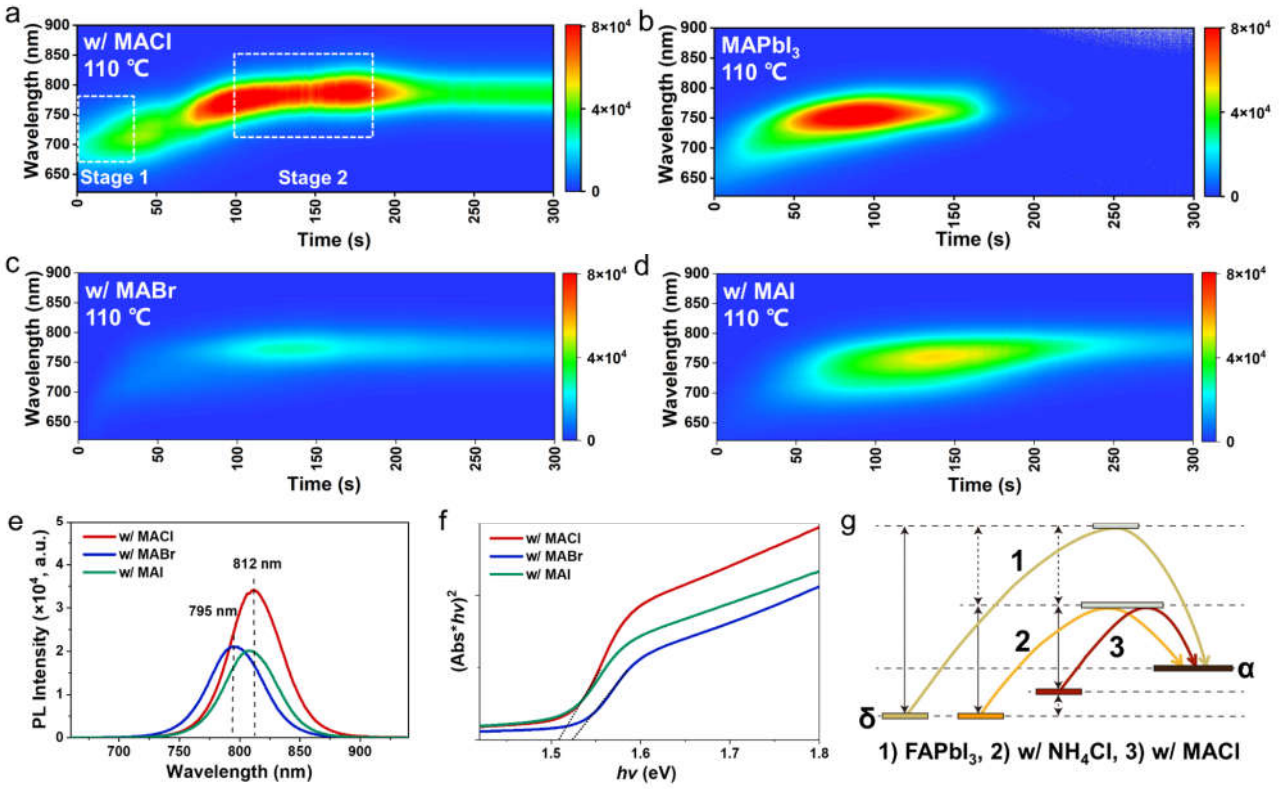

Figure 3. (a, b, c, d) Heat maps of *in-situ* PL for (a) $FAPbI_3$ with MACl, (b) $MAPbI_3$, (c) $FAPbI_3$ with MABr and (d) $FAPbI_3$ with MAI under 110 ℃ annealing temperature. (e) PL spectra of $FAPbI_3$ films with MACl, MABr or MAI additive. (f) Tauc plot of $FAPbI_3$ films with MACl, MABr or MAI additive. (g) Schematic free energy for forming $FAPbI_3$ perovskites for control, with NH_4Cl or MACl additive.

To investigate the unique PL maximum peak shift caused by the addition of MACl during heating, the $MAPbI_3$ sample was tested during annealing by *in-situ* PL (**Figure 3b and S15**). We found that the $MAPbI_3$ sample also showed a similar red shift of the maximum PL peak in the first 100 s of annealing, gradually moving from 700nm to 750nm. Furthermore, the maximum PL peak intensity also reached 1×10^5. This phenomenon shows that MA should be the dominating component in the $FAPbI_3$ sample with MACl additive in the first phase transition and crystallization stage to form an MA-based intermediate nucleus to induce faster crystallization.

The perovskite precursor solution was characterized by dynamic light scattering (DLS) to verify the MA-assisted nucleation process (**Figure S17**). We found that both peaks with particle sizes between 1–10 nm and 1–10 μm in the precursor solution shifted to larger sizes as the concentration of MACl increased from 0 to 40 mol%, indicating that MACl promotes the formation and growth of crystal nuclei in the perovskite precursor solution. Furthermore, when the annealing time ranges from 30s to 300s, the characteristic peak of the α phase in the XRD pattern (**Figure S18**) moves from 14.08° to 13.97°, indicating that chloride and MA were substituted by iodide and FA during the annealing process. [21]

To further verify our speculation, the effect of MA-based non-volatile additives (MABr and MAI) was investigated on the phase transition of $FAPbI_3$ (**Figure 3c,d, S19 and S20**). The PL results showed that MABr and MAI as additives also caused a redshift of the PL maximum peak like that of $MAPbI_3$ and MACl samples, which further proved that MA-based additives could play a role in assisting nucleation in the initial stage of $FAPbI_3$ film formation and phase transition. All four samples in **Figure 3a-3d** underwent an initially increased then decreased PL intensity. The changes in PL intensity result from the balance between radiative and non-radiative recombination. In the first stage of annealing, the volatilization of the solution in the precursor film leads to supersaturation of the solute. Then, many luminating nanocrystals are formed at this stage, resulting in a gradually increased PL intensity. In the second annealing stage, there are three possible reasons for the decreased PL intensity: 1) During the growth and fusion of tiny crystals, defects are formed in grains and grain boundaries to cause significant non-radiative recombination. [44] 2) Continuous heating will form thermally activated carrier traps within the perovskite to increase non-radiative recombination. [45-46] 3) Continuous heating will also cause lattice vibration to increase the loss of excitation energy of the luminescence center. [47] As a result, the PL intensity started to decrease after reaching the peak. Further comparing the difference between volatile MACl and non-volatile MABr and MAI, we found that when the MACl sample film was heated to 100-170 s, the maximum PL peak

signal height firstly decreased and then increased, while this phenomenon didn't exist in $FAPbI_3$ samples added with MAI or MABr and $MAPbI_3$ samples. We marked the dotted square in **Figure 3a** as stage 2. At this stage, the PL peak intensity decreased slightly after reaching the maximum peak intensity like other samples. Subsequently, the maximum PL peak intensity in the MACl sample was enhanced again, indicating that it can promote the secondary crystal growth of perovskite film due to the rapid release of volatile MACl. To verify the effect of secondary crystal growth, we have monitored the changes of the w/MACl precursor film under different annealing times by SEM. The SEM results are shown in **Figure S22(a–f)**. We found that the w/MACl precursor film formed grains of 0.3–1 μm after being annealed for 30 s. With the prolonged annealing time from 30 to 180s, the tiny grains gradually merged, and the grain sizes gradually increased. During annealing for 90-180s, an obvious growth of the crystals was observed, which corresponds to stage two in the in-situ PL in **Figure 3a**. However, when heated to 300 s, excess lead iodide appeared on the perovskite surface, which may be beneficial to passivate surface defects. This phenomenon didn't appear in the non-volatile MABr and MAI samples, which once again proved that volatile MACl had a unique auxiliary nucleation and could promote the secondary crystal growth of perovskite films to obtain better $FAPbI_3$ films.

As shown in **Figure 3e**, the PL maximum peak of the obtained MACl sample was 3 nm red-shifted than that of the MAI sample and 17 nm red-shifted than that of the MABr sample. These results suggested that the volatility of MACl could maintain the narrowest bandgap while lowering the $FAPbI_3$ phase transition temperature and promoting crystallization. The narrowest bandgap and higher absorption coefficient from the Tauc plot corresponding to the UV-Vis absorption spectrum in **Figure 3f** were also consistent with the PL results.

In summary, the MA-based additives formed a mesophase-like $MAPbI_3$ perovskite during the crystallization process, which on the one hand increased the nucleation number; on the other hand, it also decreased the phase transition temperature to below 110 °C. In addition, the volatile MA-based additive (MACl) could also promote the secondary crystal growth of perovskite films, which was very significant for obtaining high-performance $FAPbI_3$-based inverted devices. As shown in **Figure 3g**, the results discussed above could be attributed to three different crystallization pathways for α-$FAPbI_3$. The first route is that the additive-free pristine $FAPbI_3$ achieves phase transition by pure internal energy, so 150 °C is required to increase the internal energy to activate the Pb and I atoms through the energy barrier. Route 2 shows a lower energy barrier due to volatile additives, taking NH_4Cl as an example. The incorporation of NH_4Cl in the precursor can decrease the δ to α phase transition temperature to below 130 °C. This phenomenon may originate from the principle like the liquid-solid interface [48-50] and template growth [51]. In other words, NH_4Cl may coordinate with Pb and be released to activate atomic movement, thereby reducing the internal energy required to achieve phase transition at 130 °C. Route 3 represents the use of MA-based volatile additives, exemplified by MACl. The introduction of MACl can form an MA-dominated intermediate core. Compared with route 2, the initial energy level of route 3 is higher, so lower internal energy (<110°C) can help to cross the energy barrier to promote phase transition.

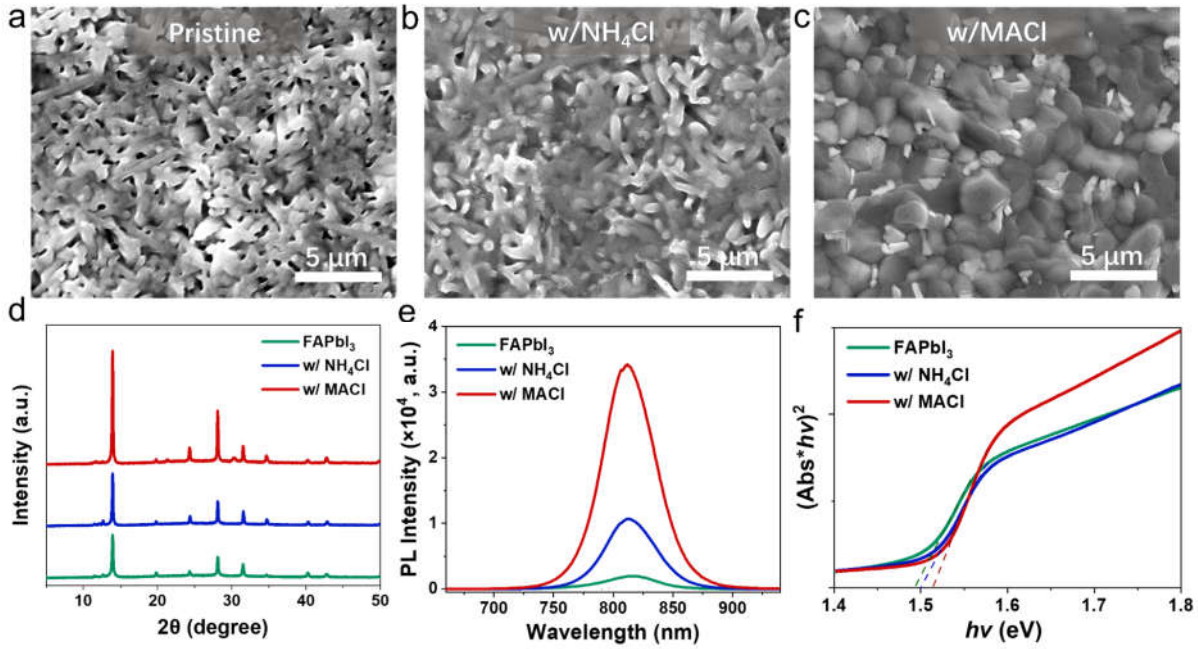

Figure 4. (a, b, c) Top-view SEM images of the $FAPbI_3$ films for (a) control, (b) with NH_4Cl and (c) with MACl. (d) The XRD patterns of $FAPbI_3$ films for control, with NH_4Cl and with MACl additive. (e) PL spectra of $FAPbI_3$ films for control, with NH_4Cl and with MACl additive. (f) Tauc plot of $FAPbI_3$ films for control, with NH_4Cl and with MACl additive.

Scanning electron microscopy (SEM) images were performed to study the morphology of $FAPbI_3$ film of three different crystallization routes. As shown in **Figure 4a**, the pristine $FAPbI_3$ film showed an average domain size of about 100 nm and some black spots, as further verified by AFM in **Figure S23**. However, the perovskite film had fewer pinholes with the incorporation of NH_4Cl (**Figure 4b**). The film became more uniform with increased grain sizes (200–400 nm), probably due to the $FAPbI_3$ growth promoted by the volatile additive. The MACl additive could also significantly increase the grain sizes to be larger than 1 μm (**Figure 4c**). The AFM measurements also verified that adding NH_4Cl and MACl additives significantly increased the grain sizes. Note that a similar phenomenon was observed in the case of $FAPbI_3$ with MABr or MAI. As shown in **Figure S18**, the $FAPbI_3$ with MABr or MAI presented a smoother surface and larger grain sizes in SEM images. The improved morphology of the perovskite with MA-based additives probably originated from the MA-rich nuclei that could regulate the crystal and growth of $FAPbI_3$ thin film. [21, 26]

X-ray diffraction (XRD) measurements were performed to study the effect of additives on the crystallinity of $FAPbI_3$ perovskite films. As illustrated in **Figure 4d**, the control film without additives showed relatively weak diffraction peaks, suggesting its poor crystallinity. Interestingly, the diffraction peak intensity was enhanced for $FAPbI_3$ film with MACl additive. The peak intensity of the (001) crystallographic plane at 14.0° in the target film with MACl was approximately two times higher than that of the control $FAPbI_3$ film, indicating its increased crystallinity in agreement with the enlarged grain size shown in the SEM images above. Photoexcited carrier behavior was investigated using steady-state photoluminescence (PL). The steady-state PL spectra in **Figure 4e** showed that PL intensity for perovskite film with MACl is over 15 times and 3 times higher than that of control and the one with NH_4Cl, respectively, indicating the suppressed nonradiative recombination. According to the Tauc plot in **Figure 4f**, The optical bandgaps were slightly affected by different volatile additives, consistent with that described in the literature. [52-53]

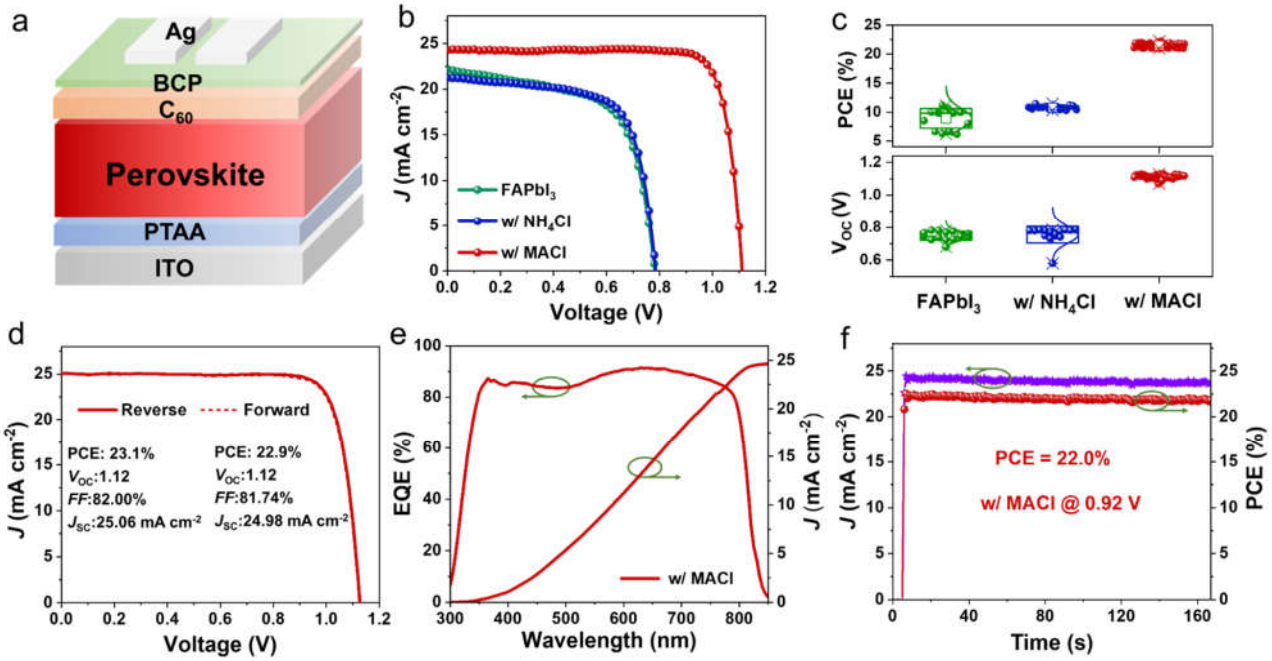

Figure 5. (a) Schematic device architecture of the inverted-structured PSC. (b) *J–V* curves of the PSCs based on $FAPbI_3$ for control, with NH_4Cl and with MACl additive. (c) Statistical PCE and V_{OC} data of the corresponding devices. (d) *J–V* curve of the best-performance PSC based on the MACl additive. (e) External quantum efficiency (EQE) spectra of the $FAPbI_3$ PSC with MACl additive. (f) The stabilized power output of the champion PSC tracked at the maximum power point (MPP) under AM 1.5G illumination.

As shown in Figure 5a, the p-i-n type inverted PSCs were fabricated with an architecture of ITO/PTAA/perovskite/C60/BCP/Ag to study the device performance of pure FAPbI3 from three crystallization routes. Figure 5b shows the current density–voltage (J–V) curves of the optimized devices. The detailed photovoltaic parameters are summarized in Table S3. The reference device based on pristine FAPbI3 showed an average PCE of 8.9% with a VOC of 0.75 V, a short-circuit current density (JSC) of 20.79 mA cm-2, and an FF of 56.24% under one sun illumination (Figure 5c, S25 and Table S3). The FF showed a significant fluctuation of ±9.73%, which should be due to the pinholes of the pristine FAPbI3 film from the SEM images above. The FAPbI3 with NH4Cl significantly increased the FF to 68.98±5.69%, resulting in an enhanced PCE of 10.79±0.32%. Furthermore, after the systematic device optimization, the MACl additive not only lowered the phase transition temperature of FAPbI3 but also achieved a higher film quality and undamaged interfaces, leading to

an average VOC of 1.11 V and a PCE of 21.46%. To fully exploit the potential of MACl additive, surface passivation and light management were further applied to improve device performance. [54] As shown in Figure 5d, the champion device based on FAPbI3 with MACl achieved a PCE of 23.1% (VOC =1.12 V, JSC=25.06 mA cm-2, and FF=82.00%), which is the highest reported for FAPbI3-based inverted PSCs (Table S1), demonstrating the great potential of MACl for enhancing device performance. To ensure data reliability, the external quantum efficiency (EQE) of the device was also measured to calibrate the cell JSC (Figure 5e). The integrated photocurrent with 24.65 mA cm-2 of the champion PSC matched well with the value obtained from the J–V measurement. A stabilized PCE of 22.0% for over 160 s was measured at maximum power point for the MACl-based PSC (Figure 5f), agreeing well with the J–V sweeps. The operational stability measured under the maximum power point (MPP) condition in **Figure S27** showed that the MACl-based device has better stability than that of pristine device in a time span of 280 hours.

CONCLUSION

In summary, this work systematically studied the functions of a series of Cl-based volatile and MA-based additives in $FAPbI_3$-based inverted PSCs. Using *in-situ* photoluminescence, we provided clear evidence to unravel the different roles of NH_4Cl and MACl in the nucleation and crystallization of $FAPbI_3$. In addition, we found that MA-based additives (MACl, MABr and MAI) could induce MA-rich nuclei to the α-phase $FAPbI_3$ compared to non-MA additives (NH_4Cl and FACl). Furthermore, volatile MACl could promote the growth of secondary crystallization during annealing. The optimized solar cell could achieve a PCE of 23.1%, which is among the best for for $FAPbI_3$-based inverted PSCs. This work provides guidance for choosing appropriate additives for achieving highly efficient inverted PSCs.

ASSOCIATED CONTENT

Supporting Information. Materials synthesis, device characterization and stability measurements. This material is available free of charge via the Internet at http://pubs.acs.org.

AUTHOR INFORMATION

Corresponding Author

*alexjen@cityu.edu.hk

Notes

The authors declare no competing financial interests.

ACKNOWLEDGMENT

A.K.Y.J. thanks the sponsorship of the Lee Shau-Kee Chair Professor (Materials Science), and the support from the APRC Grants (9380086, 9610508) of the City University of Hong Kong, the TCFS Grant (GHP/018/20SZ) and MRP Grant (MRP/040/21X) from the Innovation and Technology Commission of Hong Kong, the Green Tech Fund (202020164) from the Environment and Ecology Bureau of Hong Kong, the GRF grants (11307621, 11316422) from the Research Grants Council of Hong Kong, Shenzhen Science and Technology Program (SGDX20201103095412040), Guangdong Major Project of Basic and Applied Basic Research (2019B030302007), Guangdong-Hong Kong-Macao Joint Laboratory of Optoelectronic and Magnetic Functional Materials (2019B121205002).

REFERENCES

1. Kojima, A.; Teshima, K.; Shirai, Y.; Miyasaka, T., Organometal Halide Perovskites as Visible-Light Sensitizers for Photovoltaic Cells. *J. Am. Chem. Soc.* **2009,** *131* (17), 6050-6051.
2. Kim, H.-S.; Lee, C.-R.; Im, J.-H.; Lee, K.-B.; Moehl, T.; Marchioro, A.; Moon, S.-J.; Humphry-Baker, R.; Yum, J.-H.; Moser, J. E.; Grätzel, M.; Park, N.-G., Lead Iodide Perovskite Sensitized All-Solid-State Submicron Thin Film Mesoscopic Solar Cell with Efficiency Exceeding 9%. *Sci. Rep.* **2012,** *2* (1), 591.
3. Lee, M. M.; Teuscher, J.; Miyasaka, T.; Murakami, T. N.; Snaith, H. J., Efficient Hybrid Solar Cells Based on Meso-Superstructured Organometal Halide Perovskites. *Science* **2012,** *338* (6107), 643.
4. Luo, D.; Yang, W.; Wang, Z.; Sadhanala, A.; Hu, Q.; Su, R.; Shivanna, R.; Trindade, G. F.; Watts, J. F.; Xu, Z.; Liu, T.; Chen, K.; Ye, F.; Wu, P.; Zhao, L.; Wu, J.; Tu, Y.; Zhang, Y.; Yang, X.; Zhang, W.; Friend, R. H.; Gong, Q.; Snaith, H. J.; Zhu, R., Enhanced photovoltage for inverted planar heterojunction perovskite solar cells. *Science* **2018,** *360* (6396), 1442.
5. Kim, J. Y.; Lee, J.-W.; Jung, H. S.; Shin, H.; Park, N.-G., High-Efficiency Perovskite Solar Cells. *Chem. Rev.* **2020,** *120* (15), 7867-7918.
6. Kim, G.; Min, H.; Lee, K. S.; Lee, D. Y.; Yoon, S. M.; Seok, S. I., Impact of strain relaxation on performance of α-formamidinium lead iodide perovskite solar cells. *Science* **2020,** *370* (6512), 108.
7. De Bastiani, M.; Mirabelli, A. J.; Hou, Y.; Gota, F.; Aydin, E.; Allen, T. G.; Troughton, J.; Subbiah, A. S.; Isikgor, F. H.; Liu, J.; Xu, L.; Chen, B.; Van Kerschaver, E.; Baran, D.; Fraboni, B.; Salvador, M. F.; Paetzold, U. W.; Sargent, E. H.; De Wolf, S., Efficient bifacial monolithic perovskite/silicon tandem solar cells via bandgap engineering. *Nat. Energy* **2021,** *6* (2), 167-175.
8. Wang, K.-L.; Yang, Y.-G.; Lou, Y.-H.; Li, M.; Igbari, F.; Cao, J.-J.; Chen, J.; Yang, W.-F.; Dong, C.; Li, L.; Tai, R.-Z.; Wang, Z.-K., Smelting recrystallization of CsPbBrI2 perovskites for indoor and outdoor photovoltaics. *eScience* **2021,** *1* (1), 53-59.
9. Wu, S.; Li, Z.; Li, M.-Q.; Diao, Y.; Lin, F.; Liu, T.; Zhang, J.; Tieu, P.; Gao, W.; Qi, F.; Pan, X.; Xu, Z.; Zhu, Z.; Jen, A. K. Y., 2D metal–organic framework for stable perovskite solar cells with minimized lead leakage. *Nat. Nanotech.* **2020,** *15* (11), 934-940.
10. Chen, H.; Teale, S.; Chen, B.; Hou, Y.; Grater, L.; Zhu, T.; Bertens, K.; Park, S. M.; Atapattu, H. R.; Gao, Y.; Wei, M.; Johnston, A. K.; Zhou, Q.; Xu, K.; Yu, D.; Han, C.; Cui, T.; Jung, E. H.; Zhou, C.; Zhou, W.; Proppe, A. H.; Hoogland, S.; Laquai, F.; Filleter, T.; Graham, K. R.; Ning, Z.; Sargent, E. H., Quantum-size-tuned heterostructures enable efficient and stable inverted perovskite solar cells. *Nat. Photonics* **2022,** *16* (5), 352-358.
11. Li, X.; Zhang, W.; Guo, X.; Lu, C.; Wei, J.; Fang, J., Constructing heterojunctions by surface sulfidation for efficient inverted perovskite solar cells. *Science* **2022,** *375* (6579), 434-437.
12. Li, Z.; Li, B.; Wu, X.; Sheppard, S. A.; Zhang, S.; Gao, D.; Long, N. J.; Zhu, Z., Organometallic-functionalized interfaces for highly efficient inverted perovskite solar cells. *Science* **2022,** *376* (6591), 416-420.
13. Zeng, J.; Bi, L.; Cheng, Y.; Xu, B.; Jen, A. K. Y., Self-assembled monolayer enabling improved buried interfaces in blade-coated perovskite solar cells for high efficiency and stability. *Nano Res. Energy* **2022,** *1*, e9120004.

14. Jiang, W.; Li, F.; Li, M.; Qi, F.; Lin, F. R.; Jen, A. K. Y., π-Expanded Carbazoles as Hole-Selective Self-Assembled Monolayers for High-Performance Perovskite Solar Cells. *Angew. Chem. Int. Ed.* **2022,** *61* (51), e202213560.
15. Wu, X.; Li, B.; Zhu, Z.; Chueh, C.-C.; Jen, A. K. Y., Designs from single junctions, heterojunctions to multijunctions for high-performance perovskite solar cells. *Chem. Soc. Rev.* **2021,** *50* (23), 13090-13128.
16. Kim, M.; Jeong, J.; Lu, H.; Lee, T. K.; Eickemeyer, F. T.; Liu, Y.; Choi, I. W.; Choi, S. J.; Jo, Y.; Kim, H.-B.; Mo, S.-I.; Kim, Y.-K.; Lee, H.; An, N. G.; Cho, S.; Tress, W. R.; Zakeeruddin, S. M.; Hagfeldt, A.; Kim, J. Y.; Grätzel, M.; Kim, D. S., Conformal quantum dot–SnO2 layers as electron transporters for efficient perovskite solar cells. *Science* **2022,** *375* (6578), 302-306.
17. Min, H.; Lee, D. Y.; Kim, J.; Kim, G.; Lee, K. S.; Kim, J.; Paik, M. J.; Kim, Y. K.; Kim, K. S.; Kim, M. G.; Shin, T. J.; Il Seok, S., Perovskite solar cells with atomically coherent interlayers on SnO2 electrodes. *Nature* **2021,** *598* (7881), 444-450.
18. Fu, Q.; Liu, H.; Li, S.; Zhou, T.; Chen, M.; Yang, Y.; Wang, J.; Wang, R.; Chen, Y.; Liu, Y., Management of Donor and Acceptor Building Blocks in Dopant-Free Polymer Hole Transport Materials for High-Performance Perovskite Solar Cells. *Angew. Chem. Int. Ed.* **2022,** *61*, e202210356.
19. Hui, W.; Chao, L.; Lu, H.; Xia, F.; Wei, Q.; Su, Z.; Niu, T.; Tao, L.; Du, B.; Li, D.; Wang, Y.; Dong, H.; Zuo, S.; Li, B.; Shi, W.; Ran, X.; Li, P.; Zhang, H.; Wu, Z.; Ran, C.; Song, L.; Xing, G.; Gao, X.; Zhang, J.; Xia, Y.; Chen, Y.; Huang, W., Stabilizing black-phase formamidinium perovskite formation at room temperature and high humidity. *Science* **2021,** *371* (6536), 1359-1364.
20. Jeong, J.; Kim, M.; Seo, J.; Lu, H.; Ahlawat, P.; Mishra, A.; Yang, Y.; Hope, M. A.; Eickemeyer, F. T.; Kim, M.; Yoon, Y. J.; Choi, I. W.; Darwich, B. P.; Choi, S. J.; Jo, Y.; Lee, J. H.; Walker, B.; Zakeeruddin, S. M.; Emsley, L.; Rothlisberger, U.; Hagfeldt, A.; Kim, D. S.; Gratzel, M.; Kim, J. Y., Pseudo-halide anion engineering for alpha-FAPbI3 perovskite solar cells. *Nature* **2021,** *592* (7854), 381-385.
21. Kim, M.; Kim, G.-H.; Lee, T. K.; Choi, I. W.; Choi, H. W.; Jo, Y.; Yoon, Y. J.; Kim, J. W.; Lee, J.; Huh, D.; Lee, H.; Kwak, S. K.; Kim, J. Y.; Kim, D. S., Methylammonium Chloride Induces Intermediate Phase Stabilization for Efficient Perovskite Solar Cells. *Joule* **2019,** *3* (9), 2179-2192.
22. Du, T.; Macdonald, T. J.; Yang, R. X.; Li, M.; Jiang, Z.; Mohan, L.; Xu, W.; Su, Z.; Gao, X.; Whiteley, R.; Lin, C. T.; Min, G.; Haque, S. A.; Durrant, J. R.; Persson, K. A.; McLachlan, M. A.; Briscoe, J., Additive-Free, Low-Temperature Crystallization of Stable alpha-FAPbI3 Perovskite. *Adv. Mater.* **2022,** *34* (9), e2107850.
23. Zhang, D.; Zhang, H.; Guo, H.; Ye, F.; Liu, S.; Wu, Y., Stable α-FAPbI3 in Inverted Perovskite Solar Cells with Efficiency Exceeding 22% via a Self-Passivation Strategy. *Adv. Funct. Mater.* **2022,** *32* (27).
24. Jiang, Q.; Tong, J.; Xian, Y.; Kerner, R. A.; Dunfield, S. P.; Xiao, C.; Scheidt, R. A.; Kuciauskas, D.; Wang, X.; Hautzinger, M. P.; Tirawat, R.; Beard, M. C.; Fenning, D. P.; Berry, J. J.; Larson, B. W.; Yan, Y.; Zhu, K., Surface reaction for efficient and stable inverted perovskite solar cells. *Nature* **2022,** *611* (7935), 278-283.
25. Cui, X.; Jin, J.; Tai, Q.; Yan, F., Recent Progress on the Phase Stabilization of FAPbI3 for High-Performance Perovskite Solar Cells. *Solar RRL* **2022,** *6* (10), 2200497.
26. Zhang, Y.; Li, Y.; Zhang, L.; Hu, H.; Tang, Z.; Xu, B.; Park, N.-G., Propylammonium Chloride Additive for Efficient and Stable FAPbI3 Perovskite Solar Cells. *Adv. Energy Mater.* **2021,** *11* (47), 2102538.
27. Lu, H.; Liu, Y.; Ahlawat, P.; Mishra, A.; Tress, W. R.; Eickemeyer, F. T.; Yang, Y.; Fu, F.; Wang, Z.; Avalos, C. E.; Carlsen, B. I.; Agarwalla, A.; Zhang, X.; Li, X.; Zhan, Y.; Zakeeruddin, S. M.; Emsley, L.; Rothlisberger, U.; Zheng, L.; Hagfeldt, A.; Gratzel, M., Vapor-assisted deposition of highly efficient, stable black-phase FAPbI3 perovskite solar cells. *Science* **2020,** *370* (6512).
28. Lyu, M.; Park, N.-G., Effect of Additives AX (A = FA, MA, Cs, Rb, NH_4, X = Cl, Br, I) in $FAPbI_3$ on Photovoltaic Parameters of Perovskite Solar Cells. *Solar RRL* **2020,** *4* (10).
29. Lee, M. M.; Teuscher, J.; Miyasaka, T.; Murakami, T. N.; Snaith, H. J., Efficient Hybrid Solar Cells Based on Meso-Superstructured Organometal Halide Perovskites. *Science* **2012,** *338* (6107), 643-647.
30. Williams, S. T.; Zuo, F.; Chueh, C.-C.; Liao, C.-Y.; Liang, P.-W.; Jen, A. K. Y., Role of Chloride in the Morphological Evolution of Organo-Lead Halide Perovskite Thin Films. *ACS Nano* **2014,** *8* (10), 10640-10654.
31. Zheng, D.; Pauporté, T., Control of the quality and homogeneity of halide perovskites by mixed-chloride additives upon the film formation process. *J. Mater. Chem. A* **2021,** *9* (33), 17801-17811.
32. Zheng, D.; Zhu, T.; Pauporté, T., A Coadditive Strategy for Blocking Ionic Mobility in Methylammonium-Free Perovskite Solar Cells and High-Stability Achievement. *Solar RRL* **2021**, 2100010.
33. Ye, F.; Ma, J.; Chen, C.; Wang, H.; Xu, Y.; Zhang, S.; Wang, T.; Tao, C.; Fang, G., Roles of MACl in Sequentially Deposited Bromine-Free Perovskite Absorbers for Efficient Solar Cells. *Adv. Mater.* **2021,** *33* (3), e2007126.
34. Zhou, Y.; Herz, L. M.; Jen, A. K. Y.; Saliba, M., Advances and challenges in understanding the microscopic structure–property–performance relationship in perovskite solar cells. *Nat. Energy* **2022,** *7* (9), 794-807.
35. Stoumpos, C. C.; Malliakas, C. D.; Kanatzidis, M. G., Semiconducting Tin and Lead Iodide Perovskites with Organic Cations: Phase Transitions, High Mobilities, and Near-Infrared Photoluminescent Properties. *Inorg. Chem.* **2013,** *52* (15), 9019-9038.
36. Jeong, M.; Choi, I. W.; Go, E. M.; Cho, Y.; Kim, M.; Lee, B.; Jeong, S.; Jo, Y.; Choi, H. W.; Lee, J.; Bae, J.-H.; Kwak, S. K.; Kim, D. S.; Yang, C., Stable perovskite solar cells with efficiency exceeding 24.8% and 0.3-V voltage loss. *Science* **2020,** *369* (6511), 1615-1620.
37. Kim, G.; Min, H.; Lee, K. S.; Lee, D. Y.; Yoon, S. M.; Seok, S. I., Impact of strain relaxation on performance of α-formamidinium lead iodide perovskite solar cells. *Science* **2020,** *370* (6512), 108-112.
38. Kim, M.; Choi, I.-w.; Choi, S. J.; Song, J. W.; Mo, S.-I.; An, J.-H.; Jo, Y.; Ahn, S.; Ahn, S. K.; Kim, G.-H.; Kim, D. S., Enhanced electrical properties of Li-salts doped mesoporous TiO2 in perovskite solar cells. *Joule* **2021,** *5* (3), 659-672.
39. Lee, S.-H.; Jeong, S.; Seo, S.; Shin, H.; Ma, C.; Park, N.-G., Acid Dissociation Constant: A Criterion for Selecting Passivation Agents in Perovskite Solar Cells. *ACS Energy Lett.* **2021**, 1612-1621.
40. Park, B.-w.; Kwon, H. W.; Lee, Y.; Lee, D. Y.; Kim, M. G.; Kim, G.; Kim, K.-j.; Kim, Y. K.; Im, J.; Shin, T. J.; Seok, S. I., Stabilization of formamidinium lead triiodide α-phase with isopropylammonium chloride for perovskite solar cells. *Nat. Energy* **2021,** *6* (4), 419-428.
41. Xie, F.; Chen, C.-C.; Wu, Y.; Li, X.; Cai, M.; Liu, X.; Yang, X.; Han, L., Vertical recrystallization for highly efficient and stable formamidinium-based inverted-structure perovskite solar cells. *Energy Environ. Sci.* **2017,** *10* (9), 1942-1949.
42. Blakesley, J. C.; Castro, F. A.; Kylberg, W.; Dibb, G. F. A.; Arantes, C.; Valaski, R.; Cremona, M.; Kim, J. S.; Kim, J.-S., Towards reliable charge-mobility benchmark measurements for organic semiconductors. *Org. Electron.* **2014,** *15* (6), 1263-1272.
43. Shi, D.; Adinolfi, V.; Comin, R.; Yuan, M.; Alarousu, E.; Buin, A.; Chen, Y.; Hoogland, S.; Rothenberger, A.; Katsiev, K.;

Losovyj, Y.; Zhang, X.; Dowben, P. A.; Mohammed, O. F.; Sargent, E. H.; Bakr, O. M., Low trap-state density and long carrier diffusion in organolead trihalide perovskite single crystals. *Science* **2015,** *347* (6221), 519-522.
44. Huang, T.; Tan, S.; Nuryyeva, S.; Yavuz, I.; Babbe, F.; Zhao, Y.; Abdelsamie, M.; Weber, M. H.; Wang, R.; Houk, K. N.; Sutter-Fella, C. M.; Yang, Y., Performance-limiting formation dynamics in mixed-halide perovskites. *Sci. Adv.* *7* (46), eabj1799.
45. Liu, M.; Wan, Q.; Wang, H.; Carulli, F.; Sun, X.; Zheng, W.; Kong, L.; Zhang, Q.; Zhang, C.; Zhang, Q.; Brovelli, S.; Li, L., Suppression of temperature quenching in perovskite nanocrystals for efficient and thermally stable light-emitting diodes. *Nat. Photonics* **2021,** *15* (5), 379-385.
46. Zhang, D.; Fu, Y.; Zhan, H.; Zhao, C.; Gao, X.; Qin, C.; Wang, L., Suppressing thermal quenching via defect passivation for efficient quasi-2D perovskite light-emitting diodes. *Light Sci Appl.* **2022,** *11* (1), 69.
47. Liu, S.; Fang, X.; Lu, B.; Yan, D., Wide range zero-thermal-quenching ultralong phosphorescence from zero-dimensional metal halide hybrids. *Nat. Commun.* **2020,** *11* (1), 4649.
48. Chen, L.; Yoo, J. W.; Hu, M.; Lee, S. U.; Seok, S. I., Intrinsic Phase Stability and Inherent Bandgap of Formamidinium Lead Triiodide Perovskite Single Crystals. *Angew Chem. Int. Ed. Engl.* **2022,** *61* (50), e202212700.
49. Du, T.; Macdonald, T. J.; Yang, R. X.; Li, M.; Jiang, Z.; Mohan, L.; Xu, W.; Su, Z.; Gao, X.; Whiteley, R.; Lin, C. T.; Min, G.; Haque, S. A.; Durrant, J. R.; Persson, K. A.; McLachlan, M. A.; Briscoe, J., Additive-Free, Low-Temperature Crystallization of Stable alpha-FAPbI(3) Perovskite. *Adv. Mater.* **2022,** *34* (9), e2107850.
50. Stoumpos, C. C.; Malliakas, C. D.; Kanatzidis, M. G., Semiconducting tin and lead iodide perovskites with organic cations: phase transitions, high mobilities, and near-infrared photoluminescent properties. *Inorg. Chem.* **2013,** *52* (15), 9019-38.
51. Huang, Y.; Liang, J.; Zhang, Z.; Zheng, Y.; Wu, X.; Tian, C.; Zhou, Z.; Wang, J.; Yang, Y.; Sun, A.; Liu, Y.; Tang, C.; Chen, Z.; Chen, C. C., Low-Temperature Phase-Transition for Compositional-Pure alpha-FAPbI3 Solar Cells with Low Residual-Stress and High Crystal-Orientation. *Small Methods* **2022,** *6* (11), e2200933.
52. Min, H.; Kim, M.; Lee, S.-U.; Kim, H.; Kim, G.; Choi, K.; Lee, J. H.; Seok, S. I., Efficient, stable solar cells by using inherent bandgap of α-phase formamidinium lead iodide. *Science* **2019,** *366* (6466), 749-753.
53. Ma, L.; Zhang, S.; Wang, J.; Ren, J.; Gao, M.; Zhang, J.; Zhang, T.; Yao, H.; Ye, L.; Hou, J., Miscibility Control by Tuning Electrostatic Interactions in Bulk Heterojunction for Efficient Organic Solar Cells. *ACS Mater. Lett.* **2021,** *3* (9), 1276-1283.
54. Li, F.; Deng, X.; Qi, F.; Li, Z.; Liu, D.; Shen, D.; Qin, M.; Wu, S.; Lin, F.; Jang, S.-H.; Zhang, J.; Lu, X.; Lei, D.; Lee, C.-S.; Zhu, Z.; Jen, A. K. Y., Regulating Surface Termination for Efficient Inverted Perovskite Solar Cells with Greater Than 23% Efficiency. *J. Am. Chem. Soc.* **2020,** *142* (47), 20134-20142.

Table of Contents